Impacts of Re-greening the Desertified Lands in Northwestern China: Implications from a Regional Climate Model Experiment

Article *in* Journal of the Meteorological Society of Japan · December 2004

DOI: 10.2151/jmsj.82.1679

3 authors, including:

Omer Lutfi Sen
Istanbul Technical University
37 PUBLICATIONS **595** CITATIONS
SEE PROFILE

Yuqing Wang
University of Hawai'i at Mānoa
168 PUBLICATIONS **4,940** CITATIONS
SEE PROFILE

Impacts of Re-greening the Desertified Lands in Northwestern China: Implications from a Regional Climate Model Experiment

Omer Lutfi SEN

Istanbul Technical University, Eurasia Institute of Earth Sciences, Maslak, Istanbul, Turkey

Bin WANG and Yuqing WANG

International Pacific Research Center, School of Ocean and Earth Science and Technology, University of Hawaii, Honolulu, Hawaii, USA

(Manuscript received 8 August 2003, in final form 19 August 2004)

Abstract

This paper describes a study that investigates the local and regional effects of vegetation restoration in northern China via regional climate model simulations, and reports implications for the sustainability of vegetation under the altered rainfall regime. Ensemble simulations with the current vegetation cover and an idealized re-greening scenario for a test area in northwestern China (90°–110°E and 36°–42°N) were performed using large scale boundary forcing derived from 1998. The results indicate that such re-greening has both significant local and regional effects on the atmospheric circulation and rainfall distribution.

Replacing desert and semi-desert areas with grass in the test area increases net radiation at the surface, and hence total heat flux from the surface to the atmosphere. This results in enhanced ascending motions and moisture supply to the atmosphere over the test area. Consequently, rainfall increases in the whole test area. However, the increase in rainfall largely occurs due to an increase in intensity rather than an increase in frequency. Lack of frequent rainfall, especially in the lowlands of the test area, makes it very difficult to maintain a vegetated surface. This implies that the current vegetation restoration activities will be largely limited to areas where water resources are relatively abundant, or they will depend heavily on irrigation. The increased runoff at higher elevations could be important for providing water for irrigation in the lowlands. The increase in rainfall in the highlands and far eastern parts of the test area, which already receive more frequent rainfall, may help support a restored vegetation cover in these regions.

The enhanced ascending motions over the test area are compensated by increased subsidence to the east, centered over Yellow River Delta and Shandong Peninsula, resulting in a higher-pressure and anticyclonic circulation anomaly there. Consequently, rainfall decreases at these areas. This anticyclonic anomaly provides significant northeasterly low-level anomalous winds that enhance cyclonic shear vorticity in the Yangtze River Basin and South China when they meet southwesterly monsoonal flow. This causes strong ascending anomalies over southern China and the Sichuan Basin, and increases rainfall in these regions.

Corresponding author: Omer L. Sen, ITU, Eurasia Institute of Earth Sciences, 34469 Maslak Istanbul, Turkey.
E-mail: senomer@itu.edu.tr

1. Introduction

It is broadly recognized that land-surface degradation can have significant impact on the overlying atmosphere, thus on the regional cli-

mate, as it alters the surface-atmosphere interaction processes. Desertification and deforestation are two types of land-surface degradations that have been a major research focus of the scientific community over the last two decades or so because the land areas subject to desertification and deforestation expanded rapidly during the last century (e.g., Charney et al. 1975; Dickinson and Henderson-Sellers 1988; Lean and Warrilow 1989; Shukla et al. 1990; Nobre et al. 1991; Henderson-Sellers et al. 1993; Lean and Rowntree 1993; McGuffie et al. 1995; Xue 1996; Hahmann and Dickinson 1997; Kanae et al. 2001; Zeng et al. 2002; Sen et al. 2004).

Desertification refers to land surface degradation in arid, semi-arid, and dry semi-humid areas that has resulted from human activities such as overcultivation of marginal land, unsustainable 'slash-and-burn' agricultural practice, logging for fuelwood, poor irrigation techniques, and overgrazing (Wang and Jenkins 2002). Desertification increases surface albedo, hence reducing net radiation at surface, which leads to radiative cooling of the surface. This enhances sinking motions in the atmosphere that decreases precipitation. The reduction in rainfall decreases soil moisture, which leads to a reduction in evaporative flux. Consequently, the Bowen Ratio (BR; the ratio of sensible heat flux to latent heat flux) increases, that is, atmospheric humidity decreases, which leads to a further reduction in precipitation. The change in surface temperature due to desertification is primarily related to the competing effects of the changes in albedo and latent heat flux (Wang and Jenkins 2002): an increase in albedo cools the surface, whereas a reduction in latent heat flux, especially in wet season when latent heat flux is relatively large, warms the surface. The total effect is, therefore, highly season dependent, and the surface is usually cooler in the dry season but could become warmer in the wet season.

China is one of the countries that have experienced profound desertification during the last several decades. Desertification is affecting one third of the country. Annual expansion is reaching to a rate well over 2400 km^2/year (Zhao et al. 2002). China has made plans to bring its growing land desertification under control by 2010 through massive restoration of vegetation across the country. Western China Development Plan that has been implemented in China aims to replace farmlands and regreen the desertified lands with forest and grass to fight against desertification (Shi and Wang 2003). The sustainability of the restored vegetation cover, however, remains a big question. Reversing the desertification process largely depends on a persistent increase in precipitation, especially in its frequency, to support restored vegetation.

In order to investigate whether a relatively large-scale vegetation restoration effort can improve local rainfall enough to help maintain vegetation in once desertified lands, we carried out an idealized land-cover change experiment using the International Pacific Research Center Regional Climate Model (IPRC-RegCM). We also extended the study to see how such a large-scale surface cover change affects the East-Asian summer monsoon and its rainfall.

The present paper is organized as follows. A brief introduction of the regional climate model is given in Section 2.1. The modeling experiment is described in Section 2.2. East Asian summer monsoon is briefly described in Section 2.3. The results including local changes in surface variables and regional changes in rainfall, rainfall frequency, runoff, and large-scale circulation are presented in Section 3. Conclusions are summarized in Section 4.

2. Model, experimental design, and East Asian summer monsoon

2.1 Model

The IPRC-RegCM model (Wang et al. 2003) uses hydrostatic primitive equations in spherical coordinates with sigma (pressure normalized by surface pressure) as the vertical coordinate. To facilitate accurate long-term integration, the model uses a fourth-order advective conservative finite-difference scheme (Xue and Lin 2001) on an unstaggered longitude/latitude grid system and a second-order leapfrog scheme with intermittent use of Euler backward scheme for time integration. The model has 28 vertical levels with variable resolution, the highest resolution being in the planetary boundary layer. The model physics are state-of-the-art. The comprehensive cloud microphysics scheme developed by Wang (1999, 2001) represents the grid-scale moist processes.

Subgrid convective processes, such as shallow convection, midlevel convection, and penetrative deep convection, are based on the mass-flux cumulus parameterization scheme originally developed by Tiedtke (1989) and later modified by Gregory et al. (2000). This modified version uses a CAPE closure and considers the organized entrainment and detrainment based on a simple cloud-plume model. The subgrid-scale vertical mixing is accomplished by the so-called E-ε turbulence closure scheme in which both turbulent kinetic energy and its dissipation rate are prognostic variables (Detering and Etling 1985). Surface fluxes over oceans are calculated based on the Monin-Obukhov similarity theory (Wang 2002). The radiation package was originally developed by Edwards and Slingo (1996) and further improved by Sun and Rikus (1999). Cloud amount is diagnosed by using the semi-empirical cloudiness parameterization scheme developed by Xu and Randall (1996) based on the results from cloud-resolving model simulations.

For the land-surface processes, the model uses the Biosphere-Atmosphere Transfer Scheme (BATS) developed by Dickinson et al. (1993). BATS incorporates one canopy and three soil layers, and it requires land cover/vegetation (18 types), and soil texture (12 types) maps for spatial applications as in a GCM. In our application, these datasets were obtained from the U.S. Geological Survey (the second version of the USGS 1-km resolution land-cover classification dataset), and the U.S. Department of Agriculture (global 10-km soil data). Similar to most other grid-point regional climate models, a one-way nesting is used to update the model time-integration in a buffer zone near the lateral boundaries within which the model prognostic variables are nudged to the reanalysis data with a linear nudging coefficient.

2.2 *Experimental design*

The IPRC-RegCM was used to carry out two ensemble simulations, each with 5 members with different initial conditions spanning 5 days centered on April 20, 1998. The current surface cover was used in one ensemble (hereafter CURRENT) while a re-greening scenario in another (hereafter GRASS). The CURRENT simulations are the same as the control simulations used in Sen et al. (2004). In the GRASS simulations, the grids with the "desert" and "semi-desert" land-cover classes of BATS—those falling between 90°–110°E and 36°–42°N (referred as "test area" in this paper; see the box in Fig. 1)—were replaced with the "short grass" vegetation class. The test area involves serious vegetation restoration efforts supported by the government of China (Shi and Wang 2003).

Table 1 gives some of the parameters and their values associated with the above-mentioned three land-cover/vegetation classes in BATS. By definition in BATS, maximum fractional vegetation cover can be as high as 0.80 for grass, but zero for desert and only 0.10 for semi-desert. The large value assigned to the parameter—fraction of water extracted by upper-layer roots (see Table 1)—indicates that grass depends heavily on soil moisture in this relatively thin soil layer. The layer can quickly dry in dry conditions, and imposes large stress on vegetation that significantly limits transpiration. Albedo of grass is smaller than that of desert, but, in wet soil conditions, albedo of desert can have values as small as those of vegetated surfaces. Roughness of soil surface is 0.05 m in BATS. Roughness of grass is also assigned the same value. A larger roughness (0.10 m) is assigned to vegetation in semi-desert "biomes" in BATS.

In the experiments described above, the European Center for Medium Weather Forecasts (ECMWF) global analysis data, available at 12 h intervals with a resolution of 2.5° × 2.5° in the horizontal and 15 pressure levels up to 10 hPa, were used to define the driving fields, which provide both initial and lateral boundary conditions to the regional climate model. Sea surface temperatures (SSTs) over the ocean were obtained from the Reynolds weekly SST data with horizontal resolution of 1° × 1° (Reynolds and Smith 1994), and were interpolated into the model grids by cubic spline interpolation in space and linearly in time. Soil moisture fields were initialized in such a way that the initial soil moisture depends on the vegetation and soil type defined for each grid cell (depth of soil × field capacity × porosity).

The model domain (see Fig. 1) covers the area between 0°N–55°N, 80°E–140°E with a horizontal grid spacing of 0.5°, thus including 121

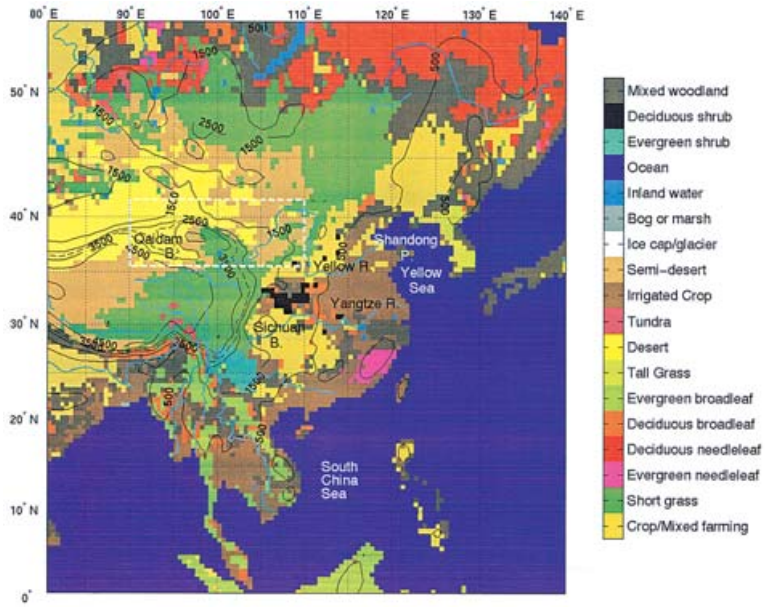

Fig. 1. BATS vegetation cover in the model domain. Contours are showing the topography. The dashed contour delineates 3000 m, which is arbitrarily used to separate "lowlands" from "highlands". The dashed rectangle is the area where "desert" and "semi-desert" grid cells are replaced with "short grass".

Table 1. Some of the parameters and their values for desert, semi-desert, and grass land cover/vegetation types in BATS.

	Desert	Semi-Desert	Grass
Maximum fractional Vegetation cover	0.0	0.10	0.80
Roughness Length (m)	0.05	0.10	0.05
Depth of the upper soil layer (mm)	100	100	100
Depth of the rooting zone soil layer (mm)	1000	1000	1000
Fraction of water extracted by upper layer roots (saturated)	0.90	0.80	0.80
Vegetation albedo for wavelengths < 0.7 μm	0.20	0.17	0.10
Vegetation albedo for wavelengths > 0.7 μm	0.40	0.34	0.30

by 111 grid points. The USGS high-resolution topographic dataset ($0.0833° \times 0.0833°$) was used to obtain the model topography (Fig. 1). The high-resolution vegetation type data from USGS is reanalyzed to represent the dominant vegetation type in each grid box, except in the GRASS experiment in which the grid cells with "desert" and "semi-desert" types in the test area were just replaced with "short grass". In addition to model domain, land cover/vegetation type and topography, Fig. 1 shows the approximate locations of the places that are often referred in the text. The dashed 3000-m contour in the figure separates for demonstration purposes "highlands" or "higher elevations" (> 3000 m) from "lowlands" or "lower elevations" (< 3000 m) in the test area, these words being frequently used in the text to show the fairly different responses these regions give to the modeled land cover change.

The model simulations were initialized from 00Z on April 20, 1998, and integrated continuously through August 31. The results are reported in terms of the averages of each ensemble. As reported briefly in the next section,

1998 had a wet summer with floods in Yangtze River. In that sense, this experiment quantifies the regional effects of the aforementioned surface cover change for an extreme wet year. Although it is difficult to generalize the results to other years (i.e., climatology), the results are still relevant as they may represent wet years that have very important consequences for the region, such as flooding.

2.3 The 1998 East Asian summer monsoon

Because the present study investigates the effect of northern China's re-greening on the East Asian summer monsoon (EASM), we will provide a brief description of the EASM and its 1998 evolution. Detailed information can be found in Ding (1994), Ding and Liu (2001), and Wang et al. (2003). Ding (1994) identifies three airflows in the lower troposphere that cause and affect monsoon processes over East Asia: The Indian monsoonal westerlies, which carry abundant moisture from the Indian Ocean; the cross-equatorial airflow over northern Australia and its neighboring sea region; and the tropical western Pacific easterlies associated with the western Pacific subtropical high pressure system (WPSH).

The onset of the EASM is widely recognized by the appearance of the westerlies over the South China Sea region around mid-May. As the summer monsoon develops, the primary rain belt over East Asia advances northward. This seasonal rain belt becomes somewhat stationary over South China, the Yangtze-Huaihe River Basin and North China, respectively, during its two notable northward jumps (Ding and Liu 2001). When the monsoon rainband reaches the Yangtze-Huaihe River Basin in the first half of June, it marks the beginning of the so-called Mei-Yu season in China (Wang and LinHo 2002). The Mei-Yu season, which peaks in late June, is characterized by persistent and torrential rainfall associated with the quasi-stationary Mei-Yu front. The withdrawal of the monsoon rainy season from China occurs in late August.

The summer of 1998 was marked with heavy rainfalls that caused severe floods (eight flood peaks between June and September) in the Yangtze River Basin, the largest since 1954 summer. More than 3000 deaths and large economic losses in China were associated with these floods. An unusual second Mei-Yu period occurring in the 1998 summer (Ding and Liu 2001) was believed to increase the losses significantly. The abnormal monsoon rainfall was also related to the prolonged impact of the 1997–1998 El Nino event, which was the strongest in the last century (Wang et al. 2000).

3. Results

3.1 Model performance

The performance of the model was primarily assessed through its ability to simulate spatial and temporal variations in rainfall, as rainfall is a stringent criterion and the main concern in this study. A gridded version of the daily rainfall data from approximately 950 stations (most of them in China, the Korean Peninsula, Mongolia, Thailand and Vietnam) was utilized to evaluate the model simulations. Because the statistics related to control simulations (CURRENT) are published in Sen et al. (2004), readers are referred to that publication in order to avoid repetition in the present paper. As mentioned there, the model simulated well the majority of the precipitation events associated with both southward propagating cold frontal systems and the quasi-stationary Mei-Yu fronts. The overall performance of the model is, therefore, deemed adequate to carry out this sensitivity study.

3.2 Local changes

As mentioned earlier, re-greening the desertified lands is expected to change the local weather and climate through altering exchanges of energy, water vapor and momentum between surface and atmosphere. This section reports the changes in surface variables both temporally and spatially over the test area. Hereafter, the analysis concentrates, in general, on combined effects in June, July and August (JJA) as JJA marks the mature phase of EASM. The beginning of JJA also comes sufficiently later than the initialization date of the simulations, which lessens concerns about the model's "spin-up".

Figure 2 shows daily variations of net surface radiation, Bowen Ratio (BR), and rainfall for two ensembles averaged for the whole test area. Note that the area contains some unchanged vegetation (see Fig. 1), albeit only a small fraction. Changing the surface cover from

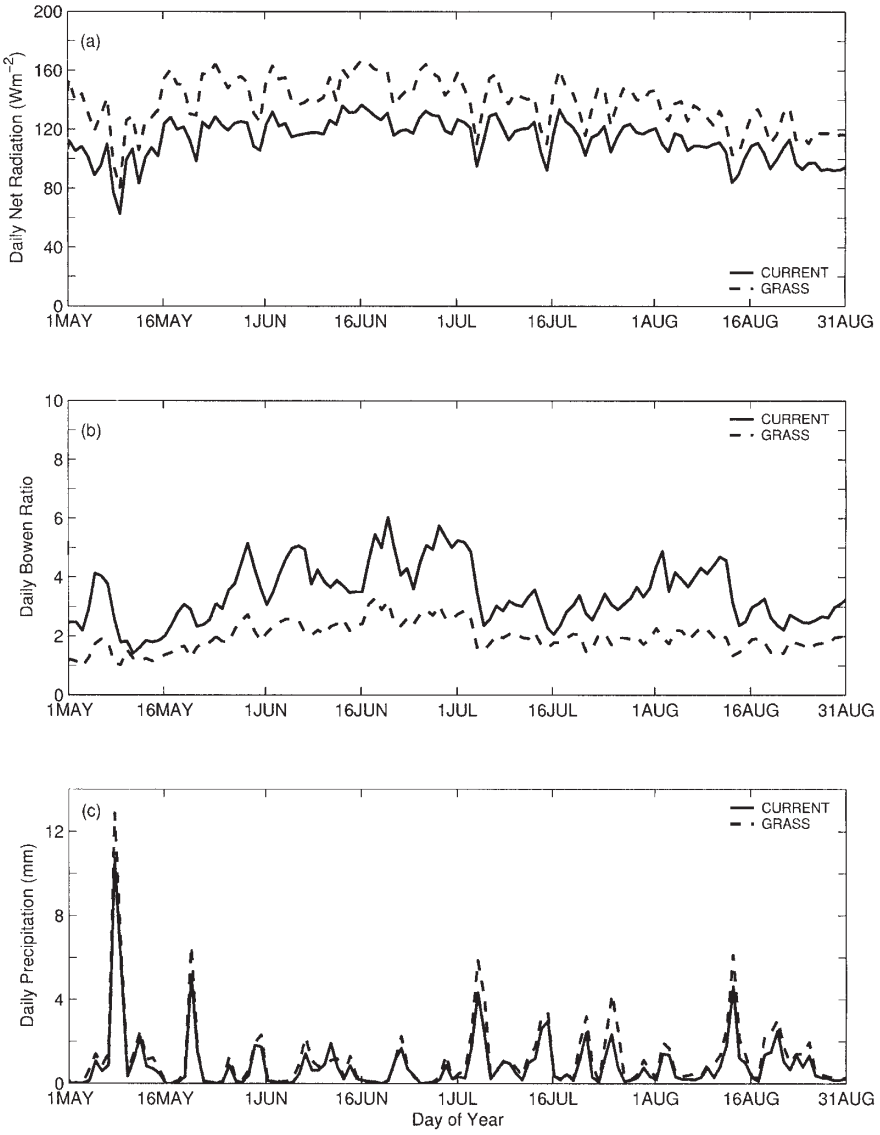

Fig. 2. Daily variations of (a) net radiation (W m^{-2}), (b) Bowen Ratio, and (c) total rainfall (mm day^{-1}) averaged over the test area. Solid line is from CURRENT, and dashed line is from GRASS ensemble.

desert or semi-desert to grass increases the net surface radiation; the magnitude of the increase persists over time because this change is mostly driven by a change in the albedo, which is a characteristic of the surface. The simulated landscape change reduces the BR over the test area, indicating moister conditions. The changes in surface fluxes (not shown here) indicate that the reduction in the area-averaged BR is a result of the increase in latent heat flux. The area-averaged sensible heat flux does not show any large change (not shown). The modeled surface change seems to increase rainfall over the test area in general, but the increase occurs mostly as enhancement of the rainfall within the rainfall generating systems.

Figure 3 shows the changes (GRASS-CURRENT) in latent heat flux, sensible heat flux, surface layer soil moisture, and air temperature (2 m) in JJA over a domain including primarily the test area. Switching to grass increases latent heat flux over most of the test

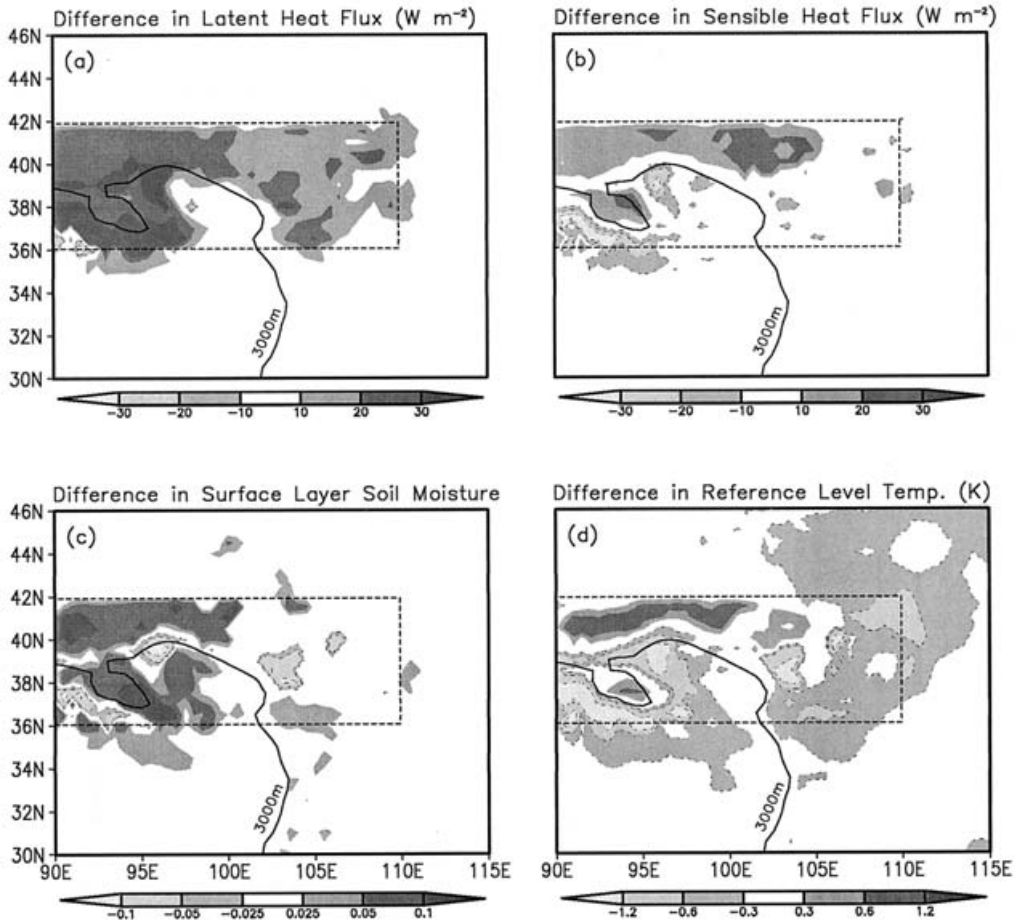

Fig. 3. Changes in (a) Latent Heat Flux (W m^{-2}), (b) Sensible Heat Flux (W m^{-2}), (c) surface layer soil moisture, and (d) 2-m air temperature (K) in JJA over a domain including mainly the test area (dashed box). For negative anomalies, dashed contours are used in addition to shading. Solid contour delineates 3000 m.

area, but the changes are not uniformly distributed, and the largest increases occur at higher elevations. Latent heat flux outside of the test area changes little (not shown). Figure 3b shows that sensible heat flux increases at lower elevations but decreases at higher elevations in the test area (probably the reason why the area-averaged sensible heat flux does not change much between two ensembles), and it does not change much outside (not shown). The changes in surface layer soil moisture (Fig. 3c), which is the main source for grass transpiration, and the changes in air temperature (Fig. 3d) depict somewhat similar patterns to that of sensible heat flux. The large positive difference in soil moisture at mostly lowlands of the test area comes from the difference in the initializations of the simulations, whereas the negative difference at high elevations is caused by rather quick recharge of the surface layer in the CURRENT simulations, in which moisture is not depleted as much as that in the GRASS simulations that is subject to higher rates of evapotranspiration. These differences can be seen better in the next two figures that provide time series of some surface variables for two areas; one at a higher and the other at a lower elevation.

Figure 4 shows daily variations in rainfall, soil moisture of both surface and rooting layers,

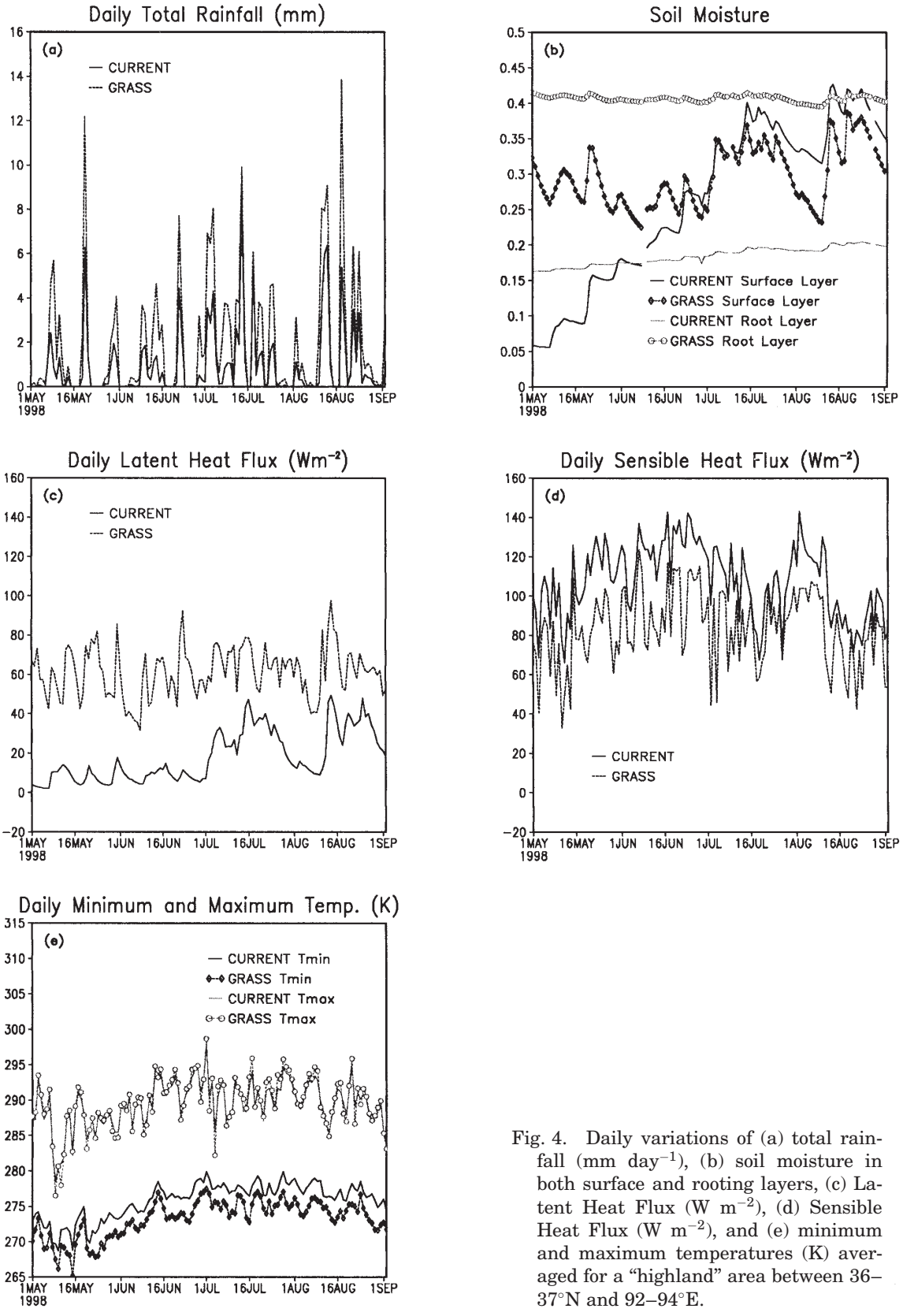

Fig. 4. Daily variations of (a) total rainfall (mm day^{-1}), (b) soil moisture in both surface and rooting layers, (c) Latent Heat Flux (W m^{-2}), (d) Sensible Heat Flux (W m^{-2}), and (e) minimum and maximum temperatures (K) averaged for a "highland" area between 36–37°N and 92–94°E.

latent heat flux, sensible heat flux, and minimum and maximum temperatures in an area between 36–36°N and 92–94°E. This area is selected to demonstrate the changes in surface variables at higher elevations in the test area. The modeled surface cover change generally increases rainfall (Fig. 4a) at higher elevations. The changes appear to be increases in the rainfall intensity within the rainfall events, and they are mostly substantial as they can amount to 40% or more over the rainfall generated in the CURRENT ensemble. The enhancement of the rainfall events may indicate a contribution from the increased local moisture as well as other atmospheric effects due to the changes in the land surface. The infiltration of rainfall into the soil clearly recharges the surface and rooting layers (Fig. 4b) in the CURRENT simulations, which then give rise to latent heat flux (Fig. 4c), especially during July and August. The soil moisture in the GRASS simulations, which is further recharged by the increased rainfall, helps the vegetated surface maintain a comparatively high amount of latent heat flux throughout the whole summer. Sensible heat flux (Fig. 4d) is reduced at high elevations, but the changes are usually smaller than those in latent heat flux.

The re-greening also lowers daily minimum temperatures but the daily maximum temperatures remain similar between the two ensembles (Fig. 4e). The decrease in albedo as a result of land-cover change leads to more net radiation to heat the surface, but it seems that the shift in energy partitioning (especially the increase in latent heat flux), which cools the surface, balances albedo effect during daytime, so the daily maximum temperatures do not differ much. The diurnal cycles of energy balance components (not shown) indicate that surface greening reduces the heat flux into the soil during daytime. Consequently, the surface becomes cooler during the night because of less heating from the soil layers below where the heat is stored during daytime. This leads to smaller daily minimum temperatures.

Figure 5 shows the same variables as in Fig. 4 but for the area between 40–41°N and 92–94°E. This area represents most of the lowlands in the test area. The area receives very little rain (Fig. 5a) indeed, and therefore, is virtually dry. Yet, switching to grass seems to increase the rainfall amount in the rainfall events significantly. It seems that the soil moisture (Fig. 5b) in GRASS ensemble drops quickly to around wilting point in the surface layer by the beginning of June. The lack of adequate rainfall to recharge soil layers results in zero latent heat flux (Fig. 5c) in the CURRENT simulations and limits latent heat flux substantially in the GRASS simulations. The daily level of latent heat flux in the latter is primarily maintained by the soil moisture in the rooting layer that shows a slow but steady decrease. Unlike at the high elevations, sensible heat flux (Fig. 5d) at the low elevations increases as, in the absence of adequate soil moisture, less energy is partitioned for evapotranspiration from the energy surplus obtained as a result of albedo decrease. Consequently, both daily minimum and maximum temperatures (Fig. 5e) become slightly higher than those in the CURRENT simulations. Note that right after the largest rainfall event (11–14 August), the daily minimum temperature from GRASS simulations falls below that from CURRENT simulations for several days.

3.3 Changes in rainfall and runoff

Figure 6 shows the changes (GRASS-CURRENT) in rainfall and whether these changes are significant at 90% confidence level. Rainfall significantly increases over the whole test area (all the hatching in the test area indicates significant increase in rainfall although the shading used in Fig. 6 does not show it because the increases are relatively small). The largest changes occur in the southern sections of the test area that have high elevations. Rainfall is also increased over the eastern flank of Tibetan Plateau, South China and the lower reaches of the Yangtze River significantly. Rainfall is significantly reduced in the northern parts of South China Sea and northern Yellow Sea. The frequency of rainfall over 16 mm day^{-1} (not shown) increases in southern China by 1–4 days $month^{-1}$, and decreases over the Shandong Peninsula and northern parts of Korean Peninsula by 1–3 days $month^{-1}$. The frequency of the rainfall less than 4 mm day^{-1} (not shown) decreases 1–4 days $month^{-1}$ over a band that extends from the test area to southern China. The largest changes occur at the high elevations of the test area, the Sichuan

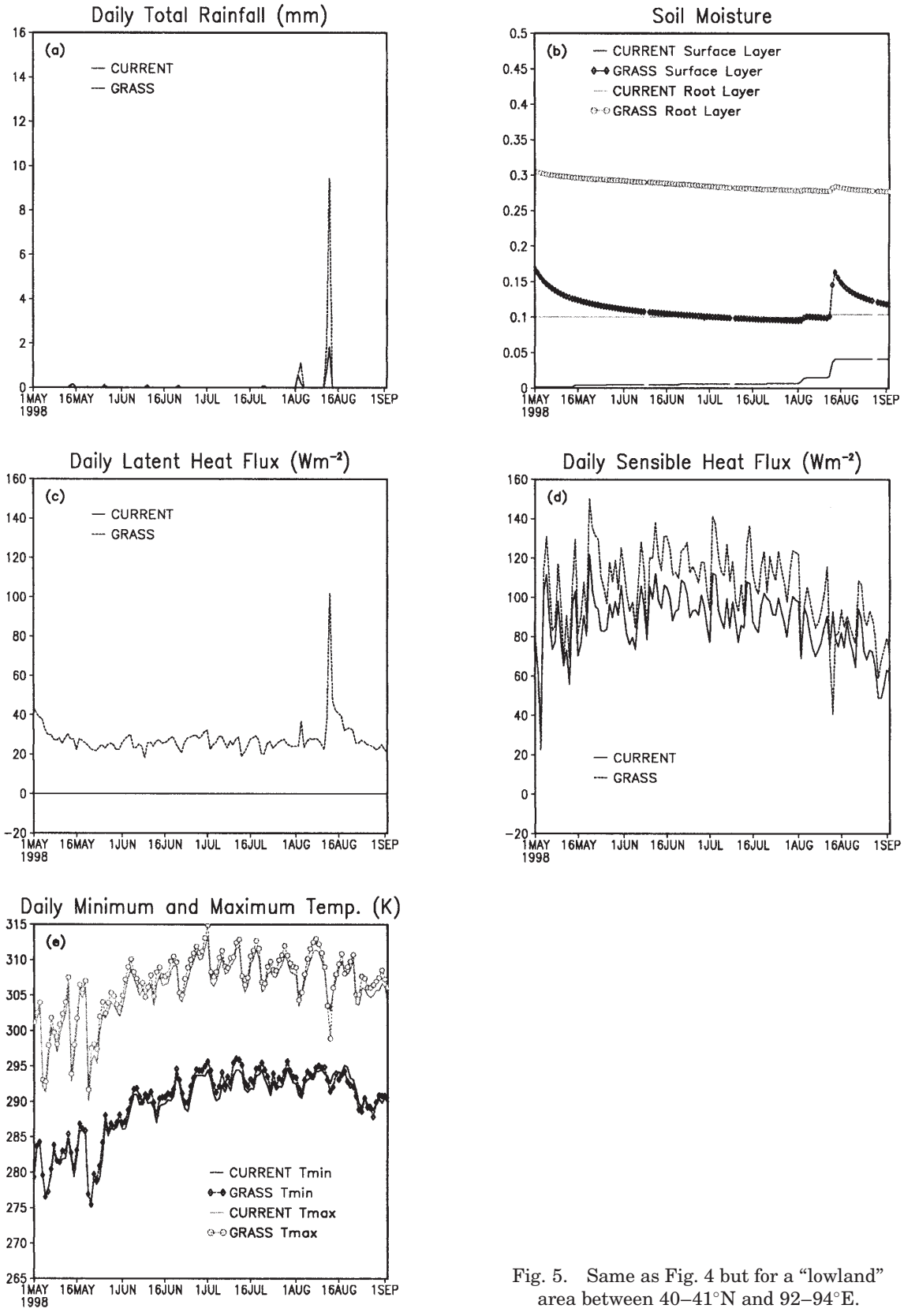

Fig. 5. Same as Fig. 4 but for a "lowland" area between 40–41°N and 92–94°E.

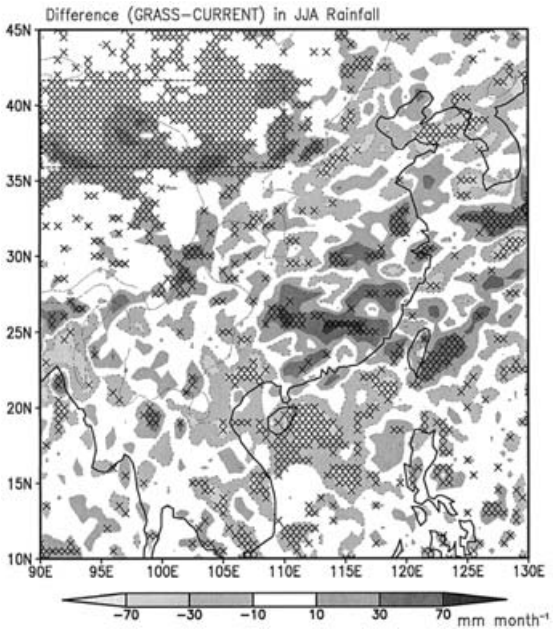

Fig. 6. Spatial distribution of rainfall change (mm month^{-1}; shaded) in JJA. For negative anomalies, dashed contours are used in addition to shading. The hatching is for statistically significant areas at 90% confidence level. The contours are showing the topography (at the 1000 and 3000 m heights). The dashed box shows the test area.

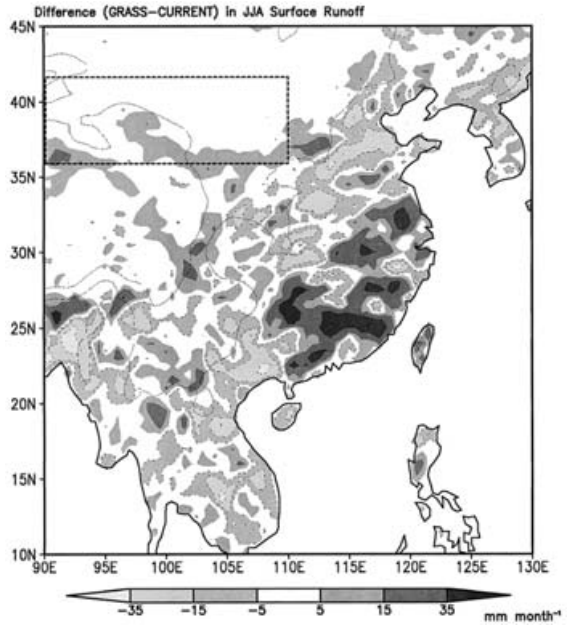

Fig. 7. Same as Fig. 6 but for surface runoff change (mm month^{-1}) in JJA.

Basin and the areas to the east. The number of days with rainfall less than 4 mm increases in the lower reaches of the Yellow River, Korean Peninsula and northern parts of Vietnam. Associated with the changes in rainfall, surface runoff (Fig. 7) increases in southern China and the lower reaches of the Yangtze River Basin and decreases in northeastern China and southwestern China.

3.4 Large-scale circulation changes

This section will focus on the description of the downstream impacts on East Asian large-scale circulation features. Figure 8 shows differences (GRASS-CURRENT) in geopotential height, wind speed, vertical velocity, and water vapor mixing ratio at three pressure levels; 500 mb, 700 mb and 850 mb. The most striking change in the large-scale circulation in the East Asian region is characterized by a dipole anomaly: a high pressure and anticyclonic anomalies located in the northern China and a low pressure and cyclonic anomalies over the southern China (Figs. 8a–c, and d–f). The northern anticyclone is centered over the Yellow River Delta, and the Shandong Peninsula, including the northern Yellow Sea and Bohai Bay (the bay to the north of Shandong Peninsula). For convenience of discussion, it will be referred to as North China high. The southern cyclone is centered over Hunan province, just south of the middle Yangtze River. For short, it will be referred to as South China low. Both of these anomalous circulation systems show an equivalent barotropic structure, in particular from the surface up to 700 hPa. The center over the 500 hPa shows a slight southward shift. Dynamically consistent with this pressure dipole, large scale descending and ascending motions occur in the North China high and South China low, respectively (Figs. 8g–i). Similarly, the moisture is depleted (accumulated) over the North China high (South China low) so that the mixing ratio shows a similar north-south dipole pattern (Figs. 8j–l).

The above changes in the large-scale atmospheric fields connect well with the changes in regional rainfall. The links between them will be discussed in the next section.

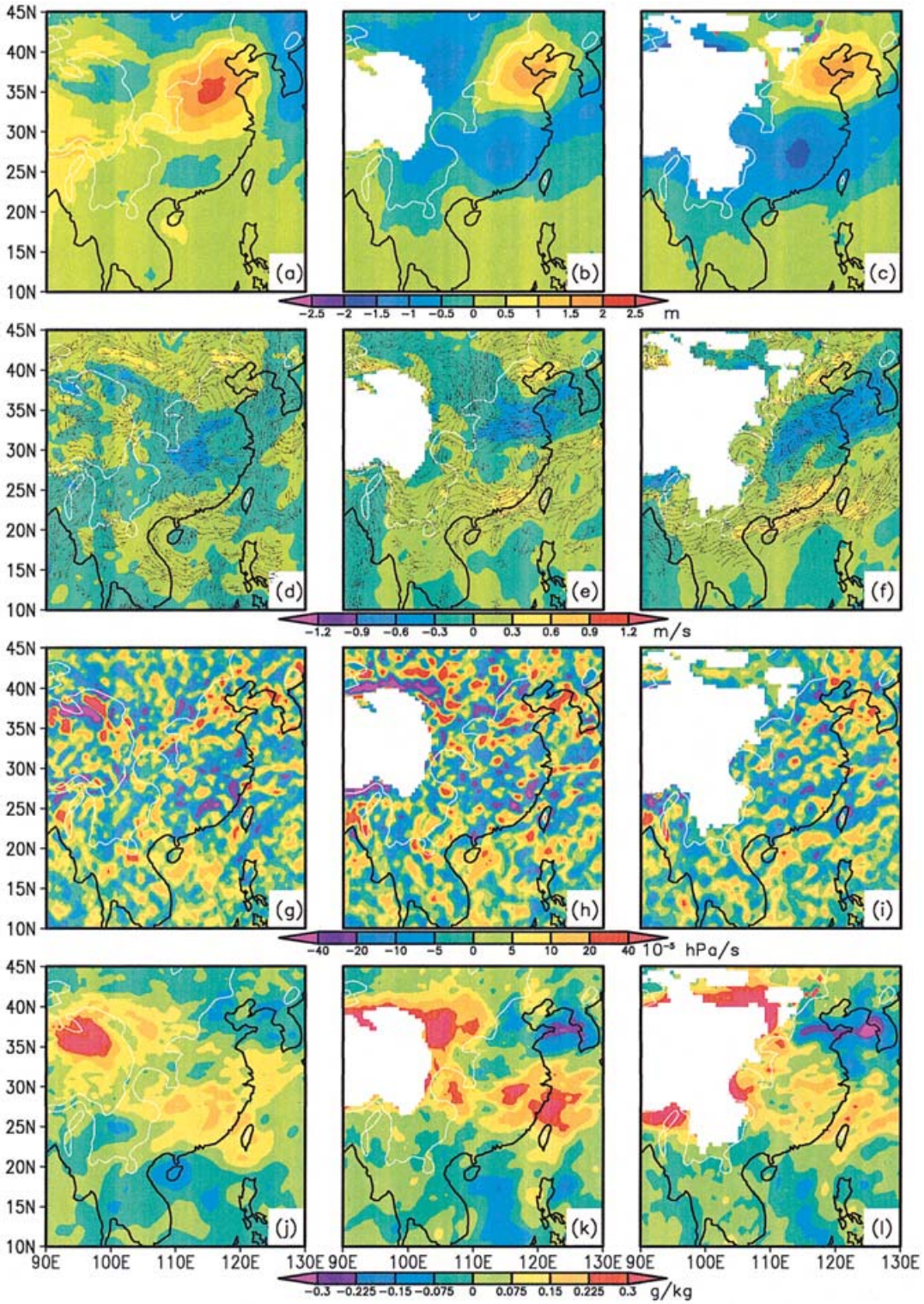

Fig. 8. Changes (GRASS-CURRENT) in geopotential height (m) of (a) 500 mb, (b) 700 mb, (c) 850 mb, in wind strength (m/s) and streamlines at (d) 500 mb, (e) 700 mb, (f) 850 mb, in vertical velocity (10^{-5} hPa/s) at (g) 500 mb, (h) 700 mb, (i) 850 mb, in water vapor mixing ratio (g/kg) at (j) 500 mb, (k) 700 mb, and (l) 850 mb in JJA. The contours are showing the topography (at the 1000 and 3000 m heights).

4. Conclusions and discussion

The present study investigates the local and regional effects of re-greening the desertified lands in northern China using a regional climate model, in particular whether the changes in rainfall induced by landscape change are large enough to support a restored vegetation cover. The results of the numerical experiment indicate that such a surface-cover change has both significant local and regional effects on rainfall and large-scale circulation. Rainfall increases significantly over the whole test area. The re-greening of the desertified lands in northwestern China increases net surface radiation in the test area. This increases total heat flux (latent heat flux plus sensible heat flux) from surface to atmosphere, which in turn enhances upward motions over the test area and supplies more moisture to the atmosphere. These two processes should primarily be responsible for the increase in precipitation over the whole test area, but owing most likely to the dynamic effect of the topography, the precipitation increases more over the higher elevations towards the Tibetan Plateau. The further cooling of the surface at higher elevations, hence overlying atmosphere, as a result of the increased latent heat flux and the decreased sensible heat flux may have contributed to increase in rainfall at the highlands. The rainfall increase in the test area seems to be associated with an increase in intensity rather than frequency whose increase at lowlands would be more valuable to support a restored vegetation cover. In general, enhanced ascending motions and more moisture transfer from soil to atmosphere appear to be the primary processes that increased rainfall in the test area.

Rainfall changes outside of the test area as well. It increases in southern China, the lower reaches of the Yangtze River, and eastern parts of the Tibetan Plateau. Significant reductions in rainfall occur mostly over the marginal seas, particularly South China and Yellow Seas. Because these remote changes should be related to the landscape change in the test area, below, we discuss a possible mechanism to link the land surface change in the test area to regional changes in rainfall. The enhancement of upward motions over the test area seems to be partly compensated by an increase in subsidence to the east over the Shandong Peninsula and Yellow River Delta, resulting in the North China high and anticyclonic circulation anomalies. The North China anticyclonic anomaly provides significant northeasterly low-level anomalous winds that stretch from the Korean Peninsula to the middle reaches of Yangtze River. This low-level flow brings relatively cold air from north and meets with southwesterly monsoon in Southeast China, enhancing cyclonic shear vorticity in the Yangtze River Basin and South China including the Sichuan Basin. The enhanced upward motions over these areas lift the moisture of monsoonal air to higher levels in the atmosphere and cause significant increases in rainfall, especially in southern China. The latent heat released in the precipitation further feedbacks to strengthen the South China low and low-level cyclonic anomalies. The moist processes enlarge the establishment of the north-south dipole pattern. Note that the development of South China low is also associated with enhanced southwesterly monsoon flow along the Southeast China coast. This low-level jet in between the western pacific subtropical high and South China low creates anticyclonic shear vorticity over the northern South China Sea, which induces descending motion and reduces rainfall there.

The results of this idealized sensitivity experiment provide important clues for the projects such as Western China Development Plan, which aims to restore vegetation in the desertified lands of China. The results suggest that reclaiming the desertified lands through vegetation restoration is quite difficult as the local climate, even after a complete vegetation restoration in a relatively large test area, can hardly support vegetation. Rainfall increases but the increase occurs in rainfall intensity and not in rainfall frequency, the latter being probably more important for the maintenance of the restored vegetation in such an environment. This implies that the current vegetation restoration activities will be largely limited to areas where water resources are relatively abundant, or they will depend heavily on irrigation. There are, however, regions in our test area that may support vegetation because they receive more frequent rainfall. These regions are mostly in the highlands towards the Tibetan Plateau and

in the eastern parts of the test area (east of 108°E), which may be a natural expansion of the eastern grasslands towards the west.

The numerical experiments in the present study were performed for only one year (1998) in which there were severe precipitation and flooding events in southern China. In this sense, the results of the experiment, particularly the regional effects. apply to that particular year, or at most, to wet years in general. Also, the experiment quantifies the local and regional effects under an idealized landscape-change scenario, which seems infeasible to that extent in practice despite serious vegetation restoration efforts in the test area that are supported by the government of China. Nevertheless, the results of the present study are very relevant as they provide important implications on the sustainability of vegetation in such an environment.

Acknowledgments

This study has been supported in part by a NASA grant to the International Pacific Research Center, which is sponsored in part by the Frontier Research System for Global Change. One of the authors, Bin Wang, acknowledges the support from NSF and NOAA/PACS program. We acknowledge the UK Met Office to allow us use its radiation scheme in the IPRC regional climate model. We appreciate the editorial assistance provided by Gisela E. Speidel, and helpful comments of two anonymous reviewers.

This paper is SOEST contribution number 6510 and IPRC contribution number 304.

References

Charney, J.G., P.H. Stone, and W.J. Quirk, 1975: Drought in the Shara: A biogeophysical feedback mechanism. *Science*, **187**, 434–435.

Detering, H.W., and D. Etling, 1985: Application of the E-, turbulence model to the atmospheric boundary layer. *Bound. Layer Meteor.*, **33**, 113–133.

Dickinson, R.E., and A. Henderson-Sellers, 1988: Modeling tropical deforestation: a study of GCM land-surface parameterization. *Quart. J. Roy. Meteor. Soc.*, **114**, 439–462.

Dickinson, R.E., A. Henderson-Sellers, and P.J. Kennedy, 1993: *Biosphere-Atmosphere Transfer Scheme (BATS) version 1e as coupled to the NCAR community climate model NCAR*. Tech. Note NCAR/TN-378+STR, 72 pp.

Ding, Y., 1994: *Monsoons over China*. Kluwer Academic Publishers, 419 pp.

Ding, Y., and Y. Liu, 2001: Onset and the evolution of the summer monsoon over the South China Sea during SCSMEX Field Experiment I 1998. *J. Meteor. Soc. Japan*, **79**, 255–276.

Edwards, J.M., and A. Slingo, 1996: Studies with a flexible new radiation code. I: Choosing a configuration for a large-scale model. *Quart. J. Roy. Meteor. Soc.*, **122**, 689–719.

Gregory, D., J.-J. Moncrette, C. Jakob, A.C.M. Beljaars, and T. Stockdale, 2000: Revision of the convection, radiation and cloud schemes in the ECMWF model. *Quart. J. Roy. Meteor. Soc.*, **126**, 2685–2710.

Hahmann, A.N., and R.E. Dickinson, 1997: RCCM2-BATS model over tropical South America: Applications to tropical deforestation. *J. Climate*, **10**, 1944–1964.

Henderson-Sellers, A., R.E. Dickinson, T.B. Durbidge, P.J. Kennedy, K. McGuffie, and A.J. Pitman, 1993: Tropical deforestation: modeling local- to regional-scale climate change. *J. Geophys. Res.*, **98**, 7289–7315.

Kanae, S., T. Oki, and K. Musiake, 2001: Impact of deforestation on regional precipitation over the Indochina Peninsula. *J. Hydrometeor.*, **2**, 51–70.

Lean, J., and D.A. Rowntree, 1993: A GCM simulation of the impact of Amazonian deforestation on climate using an improved canopy representation. *Quart. J. Roy. Meteor. Soc.*, **119**, 509–530.

Lean, J., and D.A. Warrilow, 1989: Simulation of the regional climatic impact of Amazon deforestation. *Nature*, **342**, 411–413.

McGuffie, K., A. Henderson-Sellers, H. Zhang, T.B. Durbidge, and A.J. Pitman, 1995: Global climate sensitivity to tropical deforestation. *Global and Planetary Change*, **10**, 97–128.

Nobre, C.A., P.J. Sellers, and J. Shukla, 1991: Amazonian deforestation and regional climate change. *J. Climate*, **4**, 957–988.

Reynolds, R.W., and T.M. Smith, 1994: Improved global sea surface temperature analyses using optimum interpolation. *J. Climate*, **7**, 929–948.

Sen, O.L., Y. Wang, and B. Wang, 2004: Impact of Indochina deforestation on the East-Asian summer monsoon. *J. Climate*, **17**, 1366–1380.

Shi, W., and H. Wang, 2003: The regional climate effects of replacing farmland and re-greening the desertification lands with forest or grass in west China. *Adv. Atmos. Sci.*, **20(1)**, 45–54.

Shukla, J., C. Nobre, and P.J. Sellers, 1990: Amazon deforestation and climate change. *Science*, **247**,

1322–1325.

Sun, Z., and L. Rikus, 1999: Improved application of exponential sum fitting transmissions to inhomogeneous atmosphere. *J. Geophys. Res.*, **104D**, 6291–6303.

Tiedtke, M., 1989: A comprehensive mass flux scheme for cumulus parameterization in large-scale models. *Mon. Wea. Rev.*, **117**, 1779–1800.

Wang, B., and LinHo, 2002: Rainy season of the Asian-Pacific summer monsoon. *J. Climate*, **15**, 386–398.

Wang, B., R. Wu, and X. Fu, 2000: Pacific-East Asia teleconnection: How does ENSO affect East Asian climate? *J. Climate*, **13**, 1517–1536.

Wang, G., and G.S. Jenkins, 2002: *Deserts and desertification. Encyclopedia of Atmospheric Sciences*, J.R. Holton, J.A. Curry, and J.A. Pyle, Eds., Academic Press, 633–640.

Wang, Y., 1999: *A triply nested movable mesh tropical cyclone model with explicit cloud microphysics—TCM3*. BMRC Research Report No. 74, 81pp, Bureau of Meteorology Research Center, Australia. [Available from Bureau of Meteorology Research Centre, Melbourne, Australia, VIC 3001.]

Wang, Y., 2001: An explicit simulation of tropical cyclones with a triply nested movable mesh primitive equation model—TCM3. Part I: Model description and control experiment. *Mon. Wea. Rev.*, **129**, 1370–1394.

Wang, Y., 2002: An explicit simulation of tropical cyclones with a triply nested movable mesh primitive equation model—TCM3. Part II: Model refinements and sensitivity to cloud microphysics parameterization. *Mon. Wea. Rev.*, **130**, 3022–3036.

Wang, Y., O.L. Sen, and B. Wang, 2003: A highly resolved regional climate model (IPRC_RegCM) and its simulation of the 1998 severe precipitation event over China. Part I: Model description and control experiment. *J. Climate*, **16**, 1721–1738.

Xu, K.-M., and D.A. Randall, 1996: A semiempirical cloudiness parameterization for use in climate models. *J. Atmos. Sci.*, **53**, 3084–3102.

Xue, Y., 1996: The impact of desertification in the Mongolian and the inner Mongolian grassland on the regional climate. *J. Climate*, **9**, 2173–2189.

Xue, M., and S.-J. Lin, 2001: Numerical equivalence of advection in flux and advective forms and quadratically conservative high-order advection schemes. *Mon. Wea. Rev.*, **129**, 561–565.

Zhao, J.Z., G. Wu, Y.M. Zhao, G.F. Shao, H.M. Kong, and Q. Lu, 2002: Strategies to combat desertification for the twenty-first century in China. *International Journal of Sustainable Development and World Ecology*, **9(3)**, 292–297.

Zeng, Y., G. Yu, Y. Qian, M. Miao, X. Zeng, and H. Liu, 2002: Simulations of regional climatic effects of vegetation change in China. *Quart. J. Roy. Meteor. Soc.*, **128**, 2089–2114.